PCCP

Accepted Manuscript

ROYAL SOCIETY OF CHEMISTRY

www.rsc.org/pccp

Magnetic and microwave absorption properties of self-assemblies composed of core/shell cobalt/cobalt oxides nanocrystals

Zhongzhu Wang[a,*], Hong Bi[b], Peihong Wang[a], Min Wang[a], Zhiwei Liu[a], Lei shen[a], Xiansong Liu[a]

([a] Engineering Technology Research Center of Magnetic Materials of Anhui Province, School of Physics & Materials Science, Anhui University, Hefei 230601, China)

([b] School of Chemistry and Chemical Engineering, Anhui University, Hefei 230601, China)

Abstract: Core-shell structure cobalt/cobalt oxides nanocomposites were directly synthesized via Co nanocrystals annealing in air at 300 ℃. Their microstructure and magnetic properties were characterized by XRD, TEM, XPS and VSM, respectively. The microwave absorbing properties of the nanocomposite powders dispersing in wax were investigated in 2–18 GHz frequency range. The annealing time 1 h sample exhibits the maximum reflection loss of -30.5 dB and the bandwidth less than -10 dB covering 12.6 -17.3 GHz range with the coating thickness only 1.7 mm, at the same thickness, the annealing time 3 h sample exhibits the maximum reflection loss of -24 dB and the bandwidth almost covering the whole X-band (8-11.5 GHz). With the insulating cobalt oxides shell increasing, the enhanced permeability could attribute to the decreasing of eddy current loss and the permittivity could be easily adjusted, thus, their microwave absorption properties could be easily adjusted.

Keywords: Microwave absorption; Hydrothermal synthesis; Core-shell; Cobalt/cobalt oxide; Impedance matching

1. Introduction

As an important ferromagnetic material, magnetic metal Co micro/nano particles possess high saturation magnetization and a large anisotropy field, which makes it a promising broadband microwave absorber [1-3]. During the past decades, novel Co microwave absorbers with different geometries have been steadily studied, such as

*Corresponding author. E-mail address: wangzz@ahu.edu.cn

flower-like [4], snowflake [1], hollow sphere[5, 6], and nanoplatelet[7]. Flake-shaped Co particles absorbers gain more attention due to a higher resonance frequency above Snoek's limit in the gigahertz frequency range coming from the particle shape effects [8, 9]. However, these materials still have some difficulties in increasing the permeability in the X-band (8-11.5 GHz) and Ku-band (12-18 GHz) due to the large eddy current induced by the electromagnetic wave. The strong magnetic field induced by large eddy current will cancel or dominate the external magnetic field, leading to the low permeability and poor microwave absorption properties [10, 11]. The method to overcome the eddy current loss is to make the magnetic materials be isolated in the insulator. Therefore, many nanocomposites with core@shell structures were synthesized, such as CNT/Fe[12], Co@C[13], Fe@SiO_2[14], Ni-Co-P@SiO_2[15], FeCoNi@C[16], and so on. Cao and co-workers [17, 18] have designed multiheterostructures materials such as PANI/Fe_3O_4/MWCNTs and NiO@SiC for highly effective microwave absorption, which found multi-interfaces and heterostructures played a great role in the excellent microwave absorption and increased dielectric properties. However, the chemical synthesis methods of core@shell structures usually were sophisticated, moreover, the non-magnetic shell often leads to the decreasing of saturation magnetization of the nanocomposites. Nowadays, Liu and co-workers [19]have reported the enhanced microwave properties of microporous Co@CoO nanoparticles and a relatively large reflection loss (RL) of – 90.2 dB and the bandwidth of about 7.2 GHz with RL < - 10 dB. It has been demonstrated that the proper impedance matching between complex permittivity and complex permeability can be obtained through introducing the CoO insulated shell. However, to the best of our knowledge, the method of introducing CoO shell was still sophisticated, additionally, the effect of CoO component contents on the complex permeabilities, complex permittivities and microwave absorption properties of Co/CoO composites has been seldom investigated.

Most metals are easily oxidized in air, making it simple to obtain insulated metal oxides shells [20, 21], especially, previous works on the oxidation of metal

nanoparticles, such as Ni-NiO and Co-CoO/Co_3O_4 have yielded important insights [22, 23]. Therefore, in this paper, we firstly adopt a simple method to synthesize flake-shaped assemblies composed of Co nanocrystals, then, these Co powders were directly annealed at 300 ℃ in air in order to produce proper mixtures of CoO and Co_3O_4 on the Co nanocrystals. The insulated CoO_x shells can enhance electric resistivity and the eddy current can be effectively suppressed in the X-band and Ku-band. Thus, the microwave permeability can be enhanced due to the depressing of eddy current. Additionally, the proper CoO_x shells can adjust the permittivity of Co/CoO composites because of introducing the interface polarization. At last, the complex permeability, complex permittivity and microwave absorption properties of Co/CoO_x composites embedded in the wax were investigated in the 2 – 18 GHz frequency range.

2. Experimental

In a typical procedure, 2.5 g of $CoCl_2 \cdot 6H_2O$ and 2 g CTAB were first dissolved in 15 ml of distilled water under magnetic stirring. 3 g sodium hydroxides (NaOH) were dissolved in 10 ml of distilled water, the NaOH solution and 10 ml of 85% hydrazine hydrate both were added into the above mixed solution, followed by the continual vigorous stirring for 30 min. The mixed solution was then transferred to a 50 ml Teflon-lined autoclave, which was kept at 160 ℃ for 2 h, and cooled to room temperature naturally. The Co product was collected by centrifugation, washed several times with ethanol and distilled water, and then dried at air. In the end, the dried Co particles were heated to 300 ℃ and remained at this temperature at air atmosphere for 1h ,3 h and 5 h, respectively. Then, the final product of Co/CoO_x composites were obtained and the samples were named as M-1h, M-3h and M-5h, respectively.

The microstructures and morphologies of these samples were characterized by transmission electron microscopy (TEM, JEM-2100) and X-ray powder diffraction (XRD, Japan Rigaku D/MAX-cA) using a Cu K_a radiation, respectively. X-ray photoelectron spectroscopy (XPS) was performed using an ESCA-LAB-MKII

spectrometer (VG Co., United Kingdom) with Al_{ka} X-ray radiation as the source for excitation. Magnetic hysteresis loop was measured by a vibrating sample magnetometer (VSM) (RIKEN DENSHI Co. Ltd., Japan). The as-prepared nanopowders were dispersed into wax in the mass ratio of 3:2 and compacted into rings for the permeability and permittivity measurement. The size of the ring is 7 mm in outer diameter, 3 mm in inner diameter and 3 mm in thickness. The complex permeability and complex permittivity for each sample in 2 -18 GHz range are measured based on an Agilent 8510C vector network analyzer and Agilent 85071E material measurement software. The reflection loss value (RL) for metal-backed the powders embedded in the wax coating can be calculated based on the measured complex permeability and complex permittivity at a given frequency and coating thickness according to the formula listed in the literatures [24].

3. **Results and discussion**

XRD patterns of these samples with different annealing time are shown in Fig.1, these diffraction peaks are well matched with hcp phase Co (JCPDS 05-0727), fcc phase Co (JCPDS 15-0806), cubic structure CoO (JCPDS 65-2902) and cubic structure Co_3O_4 (JCPDS 43-1003). When the Co powders were annealed in air atmosphere at 300 ℃, the mixtures of CoO and Co_3O_4 were formed. With the annealing time increasing from 1 h , 3 h to 5 h, the diffraction peak intensity of CoO phase firstly decreases and then increases. Usually, the process (Co-metal to CoO to Co_3O_4) was observed during the oxidation process [20]. However, as the annealing time increasing from 3h to 5h, the CoO phase diffraction peak becomes stronger, which maybe indicates the reverse process (Co_3O_4 to CoO to Co-metal) was simultaneous happening in the M-5h annealing process[25, 26], The above hypothesis need further investigation.

Fig.2 shows the XPS spectrum of M-3h sample, two peaks of $2P_{3/2}$ and $2P_{1/2}$ present at 779.6 eV and 794.6 eV, respectively, which are correspondence with the reported value for the Co_3O_4[27]. Additionally, the relatively strong and sharp peaks maybe indicate the mixture of Co_3O_4 and CoO [27, 28], it is noticeable that Co_3O_4 peak is

dominant for M-3 h sample, which is consistence with the XRD spectrum. The metallic Co phase is not detected from XPS spectrum, since XPS is a surface sensitive technique, it could presume that the well-coated thick shells of Co_3O_4were formed on the surface of Co particles for the M-3h sample.

Fig.3 (a) and Fig.3 (b) show the TEM image and high-resolution image (HRTEM) of annealing time 3 h sample, respectively. The TEM image clearly shows the well contrasted core/shell structure with a small cobalt dark core and a thick oxide shell. An average core diameter of 5 nm and an average shell thickness of 1.3 nm were observed. The HRTEM image shows that the core has regular lattice planes with a typical distance of 0.202 nm corresponding to the (0 0 2) planes of hcp Co, and the shell exhibits regular lattice planes with a typical distance of 0.2437 nm corresponding to the (3 1 1) planes of Co_3O_4. Although, the weak CoO phase has detected from XRD pattern of 3 h sample, the CoO structure was seldom observed in HRTEM image, which is consistence with the analysis of XPS spectrum.

Fig.4 shows the M–H hysteresis loops of the samples at room temperature. Usually, the coercivity defined as $H_c = |H_1 - H_2|/2$ and the shift is denoted by an exchange bias field defined as $H_E = |H_1 + H_2|/2$, where H_1 and H_2 are the left and right coercive fields, respectively [29]. The M-H curves do not saturate even at the highest applied field, which may be due to the existence of the disorder of magnetic spins on the surface [30]. With annealing time increasing from 1 h to 3 h and 5 h, the saturated magnetization (Ms) of the samples is 73 emu/g, 79.4 emu/g and 90 emu/g, respectively. The lower Ms value of M- 1 h sample could attribute to the existence of cobalt oxides and a higher degree of surface disorder and a lower densification stage for the powders. Increasing annealing time could not only reduce the degree of disorder of the magnetic spins at the surface but also enhance the densification of the particles, thus, the higher Ms value reached [31]. The weak H_E(2 ~3 Oe) at room temperature was both observed in M- 1h and M-5 h samples, which can attribute to the exchange interaction at the FM/AFM interface due to the existence of AFM CoO shells. However, non-existence of

exchange bias effect was observed in M-3 h sample, which can attribute to the almost non-existence (or very minor amount) of CoO phase (see Fig.1 and Fig.2). Additionally, the coercivity of the samples is 155 Oe, 182 Oe and 146 Oe, respectively. With annealing time increasing, the coercivity firstly increases then decreases. It is well known that the coercive force is influenced by many factors, such as size, structure, morphologies, etc. The coercive force increases with decrease in grain size [32], additionally, the coercive force is also proportional to the magnetic anisotropy including magnetocrystalline anisotropy, shape anisotropy and surface anisotropy [33]. The hcp-Co core itself has high coercivity due to a large magnetocrystalline anisotropy energy, with the annealing time increasing from 1 h to 3 h, the larger coercivity reached can attribute to the higher magnetocrystalline anisotropy energy due to the better crystallite. However, as the annealing time further increases to 5 h, the coercivity decreases due to both increasing the grain size and Co_3O_4 content, because of the intrinsic coercive force of Co_3O_4 is much lower than that of hcp-Co itself.

Fig. 5 shows the complex permittivity (ε', ε'') and the complex permeability (μ', μ'') of as-prepared powders embedded in wax (60 wt. % powder) in 2 – 18 GHz range. As shown in Fig.5 (a) and Fig.5 (b), for the M-1h sample, the ε' value changes between 6.4 and 14 and exhibits a maximum value at 12.8 GHz, the ε'' value shows an abrupt peak with a maximum value of 8.4 at 14.16 GHz. Apparently, the M - 3 h composite has much higher ε' values (14 ~ 18.4) than the M – 1h composite, at the meantime, the ε'' resonant peak not only shifts to the lower frequency site (11.4 GHz) but also becomes weaker. However, with annealing time further increased to the 5 h, both the ε' and the ε'' are the lowest among these samples and almost keep a constant around 9.9 and 1, respectively. Since the ion polarization and electron polarization take place at about THz and PHz, the resonance behavior of the permittivity in microwave frequency range should mainly originate from space charge polarization, dipole

polarization and interfacial polarization [19, 34]. With annealing time increasing from 1 h to 3 h, a larger quantity cobalt oxides shells in M-3h composite than in the M-1 h composite could introduce the more internal interface and decreases the electric conductivity, thus, the interface polarization and space charge polarization can both be enhanced to bring on the higher ε' value of M-3 h composite. Additionally，the twin defects comprising point defects and lattice defects were observed inside cobalt/cobalt oxides nanocrystals (see Figure 3), these defects can hinder the free electronic migration, and the higher resistance reached. Moreover, these defects can act as polarization centers, which would generate polarization relaxation under the altering electromagnetic field, the higher permittivity constant reached[12, 35]. The stronger ε'' peak of M-1h composite can attribute to the stronger eddy current loss due to the higher electric conductivity. The ε'' part usually denotes the energy loss. The ε'' peak of M-3 h composite becomes weaker and shifts to the lower frequency position due to the decrease the electric conductivity than that of M-1h composite. However, the ε' and the ε'' of M-5h composite both decrease with the annealing time further increasing to 5 h, since the intrinsic complex permittivities of cobalt oxides are much lower than those of metal Co in the microwave frequency range, thus, the far higher cobalt oxides content would decrease the permittivity of composite.

As shown in Fig.5 (c) and Fig.5 (d), for the M-1h sample, it is found the μ' is below 1.0 and the μ'' value is below zero in 12.5 – 16 GHz range, which maybe could attribute to the large eddy current induced. The strong magnetic field induced by large eddy current will cancel or dominate the external magnetic field, leading to the negative permeability [11]. Moreover, from Fig. 5(b) and (d), we can obviously see that the change trend of the permeability is just inverse to that of the permittivity. According to the Maxwell equations, a magnetic field can be induced by an ac electric field and be radiated out. So the negative μ'' denotes that the magnetic energy is radiated out and

transferred into the electric energy, which can greatly increase the ε'' and then leads to the negative μ'' [6]. For the M-3 h sample, the μ' value decreases from 1.407 to 1.11 with the frequency increase and the μ'' value has a maximum value 0.26 at 7.92 GHz. For the M-5h sample, the μ' value (1.49 ~ 1.01) and the μ'' value (~ 0.25) are observed. Apparently, with the annealing time increasing, both the μ' and μ'' increase, which could mainly contribute to the depressing of eddy current due to the decreasing of electric conductor with the more quantity cobalt oxides shells introduced. Additionally, would also have a significant influence on the high frequency magnetic properties, in nanosized magnetic particles, the spin rotation mechanism is predominant contribution to permeability in 2-18 GHz frequency range, these defects can hinder the spin rotation, thus, the high μ'' value and the large magnetic loss both reached[33].

It is well known that the magnetic loss of magnetic metal-insulator materials is mostly associated with the eddy current loss and magnetic resonance composed of domain wall resonance and natural resonance, et. al . Considering the small particle size (several nm), the domain wall resonance may be absent. If the magnetic loss only stems from the eddy current loss, the values of $\mu''(\mu')^2 f^{-1}$ should be constant when the frequency is changed, if not, the magnetic loss is ascribed to natural resonance [36]. As shown in Fig.6, We can see that the value $\mu''(\mu')^2 f^{-1}$ of M-1h sample change around 0.009 in 4 - 17 GHz, indicating the strong eddy current loss happening in the M-1h sample. However, the value $\mu''(\mu')^2 f^{-1}$ of M-3h sample and M-5h sample both decrease with the frequency increase, indicating that their magnetic loss mainly comes from natural resonance.

Fig. 7 shows the calculated refection loss (RL) of as-prepared powder embedded in wax (60 wt. % powder) coating with different thicknesses. M-1h composite exhibits the maximum RL of -30.5 dB at 14.2 GHz with the thickness of 1.7 mm and the bandwidth

less than -10 dB covering 12.6 -17.3 GHz range. M-3h composite with same thickness of 1.7mm exhibits the maximum RL of -24 dB at 10.16 GHz with the bandwidth covering 8.64 – 11.68 GHz. M-5 h composite exhibits the maximum RL of -14.5 dB at 13.68 GHz with the bandwidth covering 12.24 – 15.68 GHz. Moreover, when the coating thickness increased from 1.4 mm to 2.5 mm, the microwave absorption peaks of these samples shift to the low frequency position. The relationship between matching frequency and thickness can be expressed as following [8, 24].

$$f_m = \frac{c}{4 d_m} \frac{1}{\sqrt{\varepsilon^{'} \mu^{'}}} (1 + \frac{1}{8} \tan^2 \delta_\mu)^{-1} \quad (1)$$

where f_m is the matching frequency , d_m is the thickness and δ_μ is magnetic loss tangent. It is clear that the matching frequency decrease with increasing thickness at a given permittivity and permeability. At the same coating thickness, compared to that of M-1h composites, the matching frequency of M-3h composite shifts to the lower frequency position due to the all enhancement of permittivity, permeability and magnetic loss.

The microwave absorption properties are close corresponding to the magnetic loss, dielectric loss and impedance matching between complex permittivity and complex permeability. For the M-1h composites, the stronger absorption around 14 GHz is usually related to the stronger dielectric loss. For the M-3 h composites, the relatively strong absorption and the broad bandwidth covering the whole X-band (8-11.5 GHz) could be ascribed to the relative high dielectric loss and the enhancement of permeability and magnetic loss. For the M-5 h composites, the more excellent high frequency microwave absorption in Ku-band (12 -18 GHz) could be ascribed to the more higher permeability, the stronger magnetic loss and excellent impedance matching.

4. Conclusions

Core-shell structure cobalt/cobalt oxides nanocomposites were successfully synthesized via Co nanocrystals direct annealing in air at 300℃ for 1 h - 5 h. As annealing time increased, both the content and the thickness of cobalt oxides shells

increased, which remarkably influenced the saturation magnetization, coercive force and exchange bias of the composites. Moreover, their permeability could be improved due to the decreasing of eddy current loss with the insulating cobalt oxides shell increasing, their permittivity could be easily adjusted due to intrinsic dielectric properties and additional interface polarization of cobalt oxides shell, thus, their microwave absorption properties could be easily adjusted. M-1h sample exhibits the maximum RL of -30.5 dB and the bandwidth less than -10 dB covering 12.6 -17.3 GHz range with the thickness only 1.7 mm. M-3h sample with the coating thickness 1.7 mm exhibits the bandwidth almost covering the whole X-band. Thus, it is an effective method to adjust their microwave absorption properties and impedance matching conditions through introducing insulating cobalt oxides shells on the cobalt nanocrystals.

Acknowledgements

This work was partly supported by the National Natural Science Foundation of China (50901074, 51272002 and 51007001), Anhui Provincial Educational Ministry under Grant no. KJ2011A011, Anhui Provincial Natural Science Fund (1208085ME87 and 11040606M49), and the Young Science Foundation of Anhui University.

References

[1] F. Ma, Y. Qin, Z. Y. Li, Appl. Phys. Lett., 2010, 96, 202507.

[2]G. X. Tong, J. H. Yuan, W. H. Wu, Q. Q. Zhang, X. Cen, Q. Tang, Micro. Nano. Lett., 2012, 7, 492.

[3] T. Liu, P. H. Zhou, J. L. Xie, L. J. Deng, J. Appl. Phys., 2011, 110, 033918.

[4] Z. Ma, Q. F. Liu, J. Yuan, Z. K. Wang, C. T. Cao, J. B. Wang, Physica status solidi(b)., 2012, 249, 575.

[5] C. Z. He, S. Qiu, X. Z. Wang, J. R. Liu, L. Q. Luan, W. Liu, M. Itoh, K. I. Machida, J. Mater. Chem., 2012, 22, 22160.

[6] X. L. Shi, M. S. Cao, J. Yuan, X. Y. Fang, Appl. Phys. Lett., 2009, 95, 163108.

[7] J. G. Li, J. J. Huang, Y. Qin , F. Ma, Mater. Sci. Eng. B, 2007, 138, 199.

[8] J. Sun, H. L. Xu, Y. Shen, H. Bi, W. F. Liang, R. B. Yang, J. Alloys Comp., 2013, 548, 18.

[9] R. B. Yang, W. E. Liang, J. Appl. Phys., 2011, 109, 07A311.

[10] N. Li, C. W. Hu, M. H. Cao, Phys. Chem. Chem. Phys., 2013, 15, 7685.

[11] Z.C. Shi, R.H. Fan, Z.D. Zhang, L. Qian, M. Gao, M. Zhang, L.T. Zheng, X.H. Zhang, L.W. Yin, Adv. Mater., 2012, 24, 2349.

[12]R. C. Che, L. M. Peng, X. F. Duan, Q. Chen, X. L. Liang, Adv. Mater.,2004, 16, 401.

[13] C. H. An, Y. J. Wang, Y. N. Xu, Y. Wang, Y. N. Huang, L. F. Jiao, H. T. Yuan, Appl. Mater. Interfaces, 2014, 6, 3863.

[14] L. Yan, J. Wang, X. Han, Y. Ren, Q. Liu, F. Li, Nanotechnology, 2010, 21, 095708.

[15] Z. Ma, J. Wang, Q. Liu, J. Yuan, Appl. Mater. Interfaces, 2009, 255, 6629.

[16]F. Wen, F. Zhang, Z. Liu, J. Phys. Chem. C, 2011, 115, 14025.

[17]M. S. Cao, J. Yang, W. L. Song, D. Q. Zhang, B. W, H. B. Jin, Z. L. Hou, J. Yuan, Appl. Mater. Interfaces, 2012, 4, 6949.

[18]H. J. Yang, M. S. Cao, Y. Li, H. L. Shi, Z. L. Hou, X. Y. Fang, H. B. Jin, W. Z. Wang, J. Yuan, Adv. Optical Mater., 2014, 2, 214.

[19]T. Liu, Y. Pang, M. Zhu, S. Kobayashi, Nanoscale, 2014, 6, 2447.

[20]D. H. Ha, L. M. Moreau, S. Honrao, R. G. Hennig, R. D. Robinson, J. Phys. Chem. C, 2013, 117, 14303.

[21] J. G. Railsback, A. C. Johnston-Peck, J. Wang, J. B. Tracy, ACS Nano, 2010, 4, 1913.

[22] J. A. Medford, A. C. Johnston-Peck, J. B. Tracy, Nanoscale, 2013, 5, 155.

[23]M. Varon, I. Ojea-Jimenez, J. Arbiol, L. Balcells, B. Martinez, V. F. Puntes, Nanoscale, 2013, 5, 2429.

[24] Z. Z. Wang, J. P. Zou, Z. H. Ding, J. F. Wu, P. H. Wang, S. W. Jin, H. Bi, Mater. Chem. Phys., 2013, 142, 119-123.

[25] A. Navrotsky, C. Ma, K. Lilova, N. Birkner, Science, 2010, 330, 199.

[26] M. Martin, U. Koops, N. Lakshmi, Solid State Ionics, 2004, 172, 357.

[27]G. H. Jaffari, H. Y. Liu, C. Ni, S. I. Shah, Mater. Sci. Eng. B, 2009, 164, 23.

[28]C. L. Gao, Y. Y. Liang, M. Han, Z. Xu, J. M. Zhu, J. Phys. Chem. C, 2008, 112, 9272.

[29]S. Das, M. Patra, S. Majumdar, S. Giri, J. Alloys Comp., 2009, 488, 27.

[30]Q Ma, Y.Y. Ma, F. L. Zan, Y. F. Xu, G. H. Zheng, Z. X. Dai, M. Z. Wu, G. Li, MRS Bull., 2014, 51, 381.

[31]C.R. Vestal, Z.J. Zhang, Nano Lett., 2003, 3, 1739.

[32]M.A. Gabal, R.M. El-Shishtawy, Y.M. Al-Angari, J. Magn. Magn. Mater., 2012, 324, 2258.

[33]Z. Z. Wang, M. Z. Wu, S. W. Jin, G. Li, Y. Q. Ma, P. H. Wang, J. Magn. Magn. Mater., 2013, 344, 101.

[34]P. C. P. Watts, W. K. Hsu, A. Barnes, B. Chambers, Adv. Mater., 2003, 15, 600.

[35]C. Wang, X. J. Han, P. Xu, X. L. Zhang, Y. C. Du, S. R. Hu, J. Y. Wang, X. H. Wang, Appl. Phys. Lett., 2011, 98, 072906.

[36]F. S. Wen, H. B. Yi, L. Qiao, H. Zheng, D. Zhou, F. S. Li, Appl. Phys. Lett., 2008, 92, 042507.

Figure Captions

Figure 1. X-ray diffraction pattterns of samples obtained with annealing time 1 h, 3 h and 5 h, respectively.

Figure 2. XPS spectrum of the annealing time 3 h sample.

Figure 3. TEM image (a) and high-resolution image (b) of the annealing time 3 h sample.

Figure 4. M-H hysteresis loops of samples obtained with annealing time 1 h, 3 h and 5 h, respectively.

Figure 5. Frequency dependence of (a) real and (b) imaginary parts of complex permittivity and (c) real and (d) imaginary parts of complex permeability for the as-prepared powders/wax composite.

Figure 6. Frequency dependence of $\mu''(\mu')^2 f^{-1}$ of sample in 2 - 18 GHz.

Figure 7. Microwave reflection losses of the composites coating in 2-18 GHz.

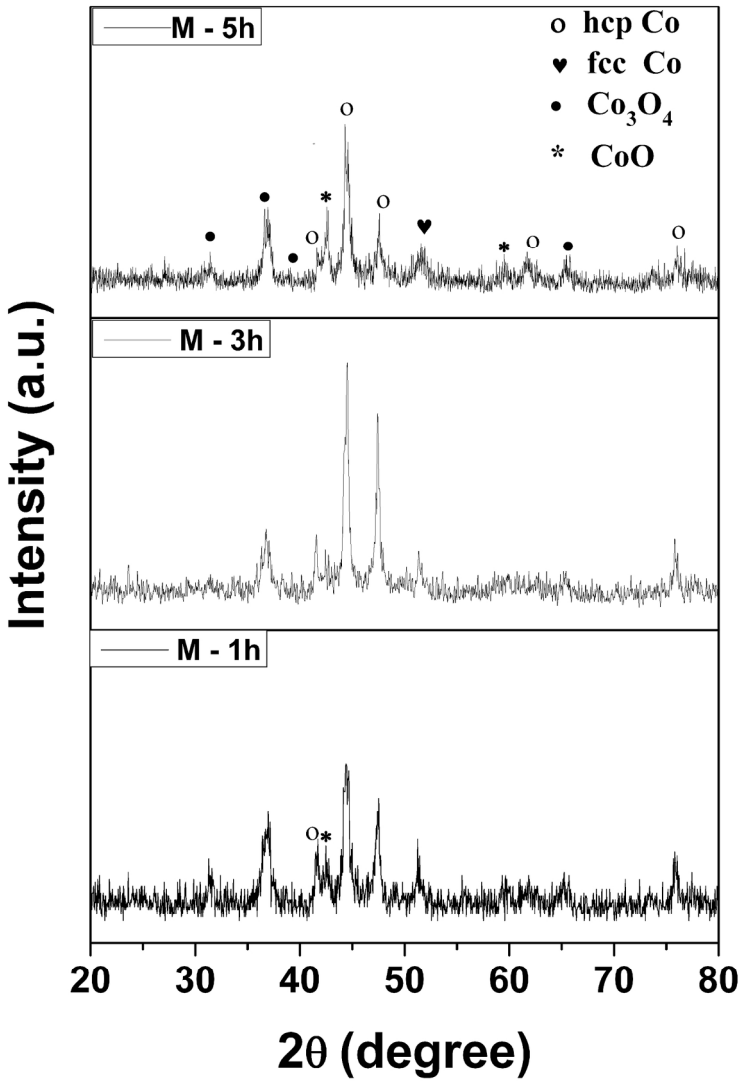

Figure 1. X-ray diffraction pattterns of samples obtained with annealing time 1 h, 3 h and 5 h, respectively.
160x229mm (300 x 300 DPI)

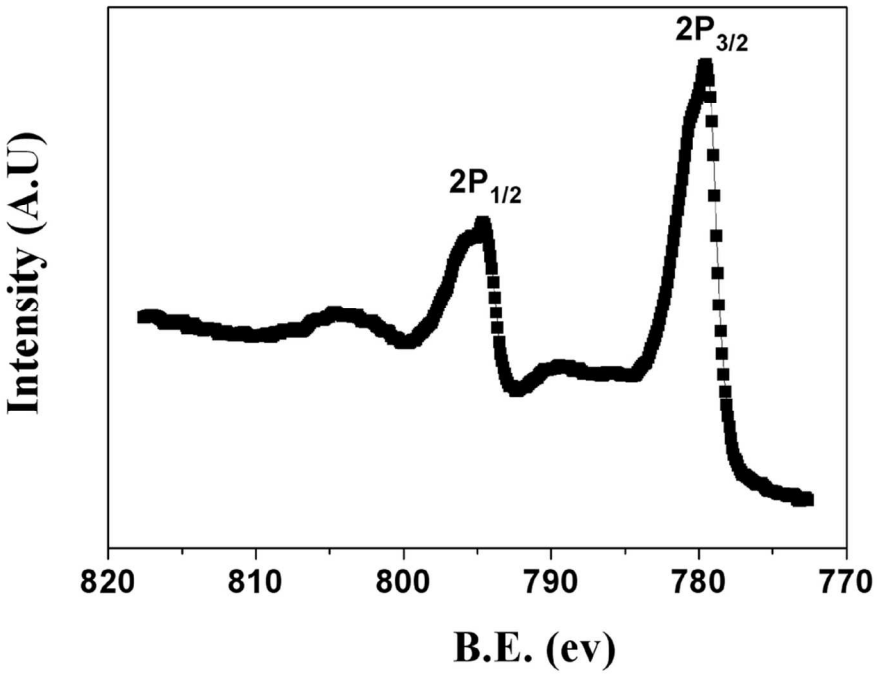

Figure 2. XPS spectrum of the annealing time 3 h sample.
99x82mm (300 x 300 DPI)

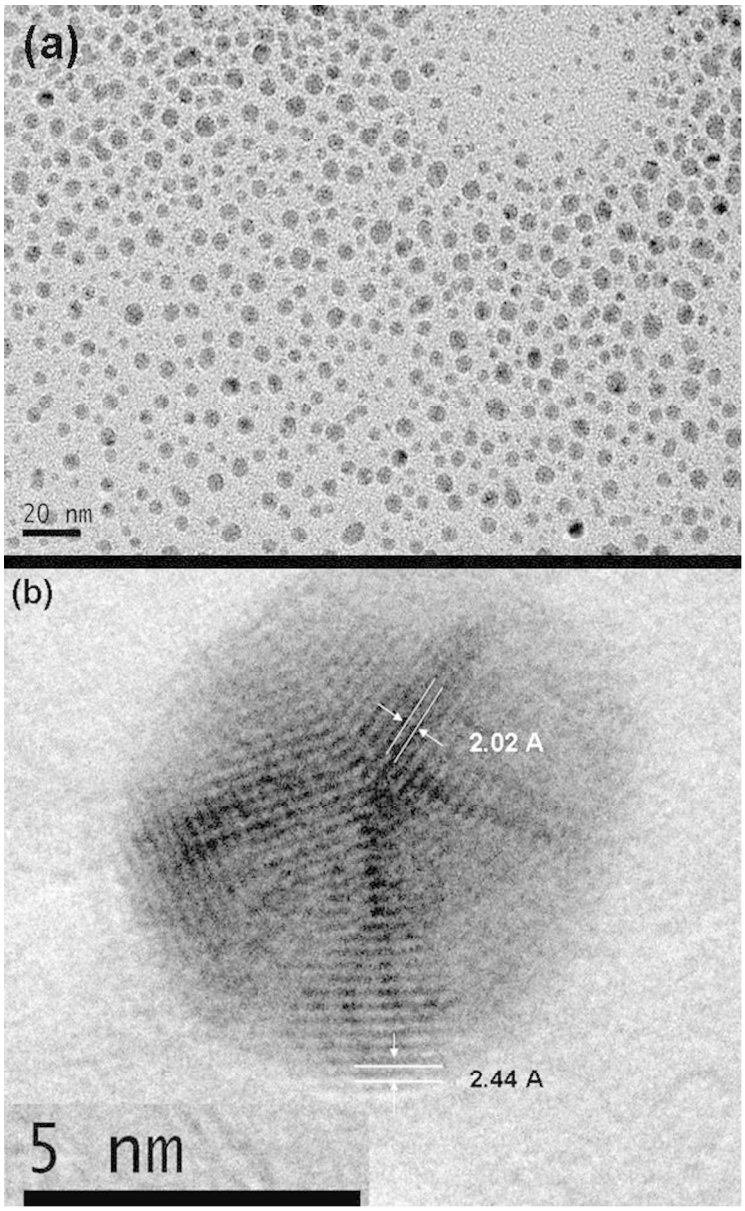

Figure 3. TEM image (a) and high-resolution image (b) of the annealing time 3 h sample.
130x211mm (600 x 600 DPI)

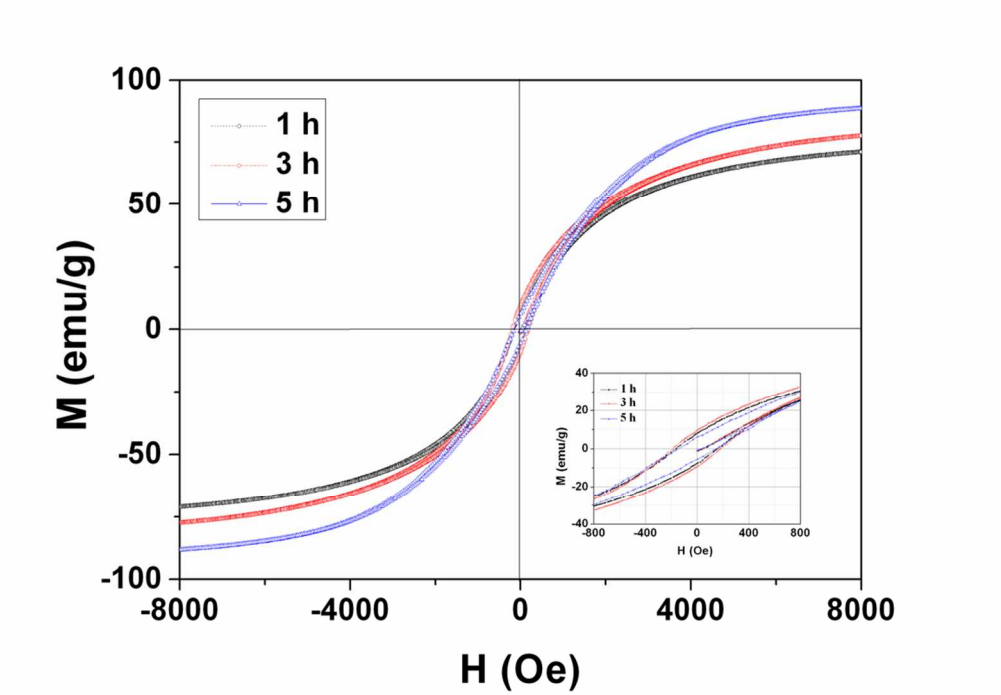

Figure 4. M-H hysteresis loops of samples obtained with annealing time 1 h, 3 h and 5 h, respectively.
97x67mm (300 x 300 DPI)

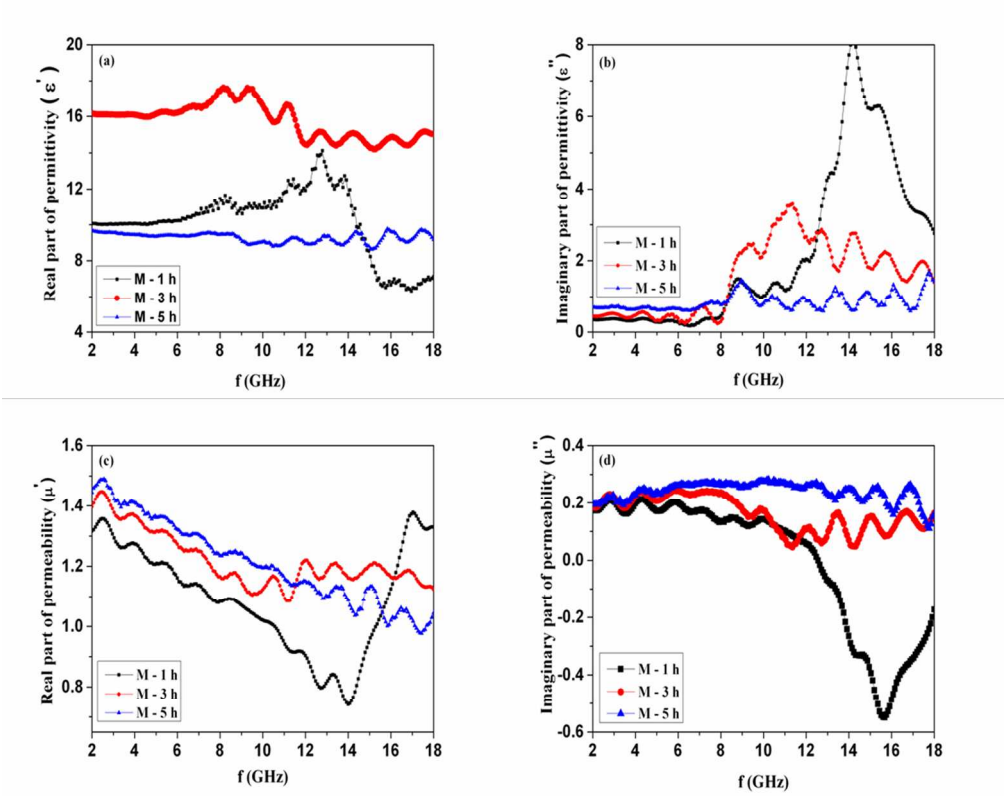

Figure 5. Frequency dependence of (a) real and (b) imaginary parts of complex permittivity and (c) real and (d) imaginary parts of complex permeability for the as-prepared powders/wax composite.
119x96mm (300 x 300 DPI)

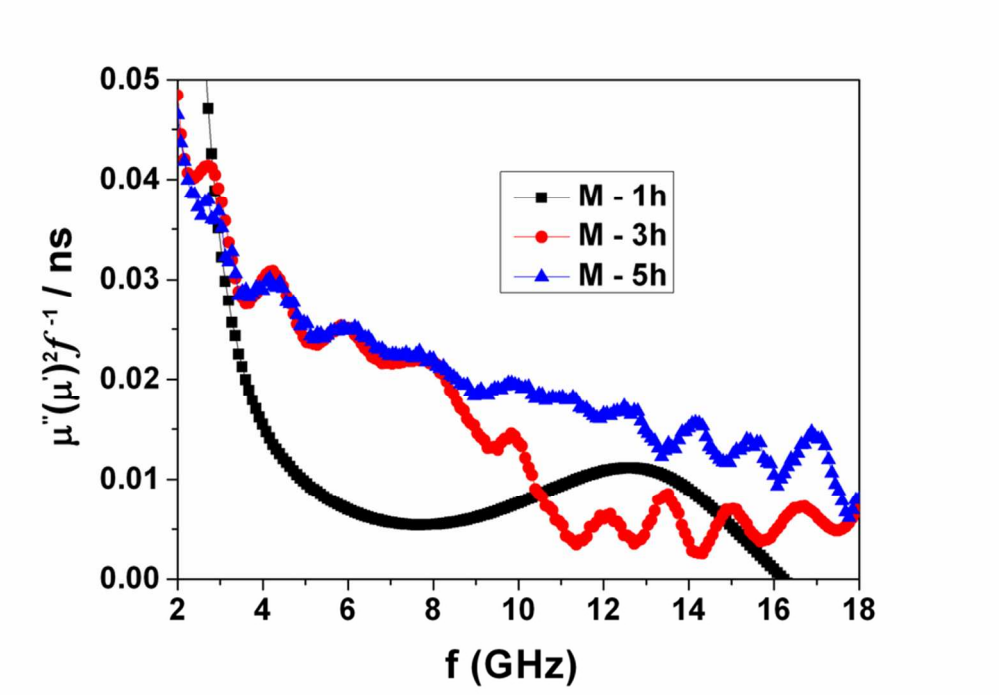

Figure 6. Frequency dependence of of sample in 2 - 18 GHz.
79x55mm (300 x 300 DPI)

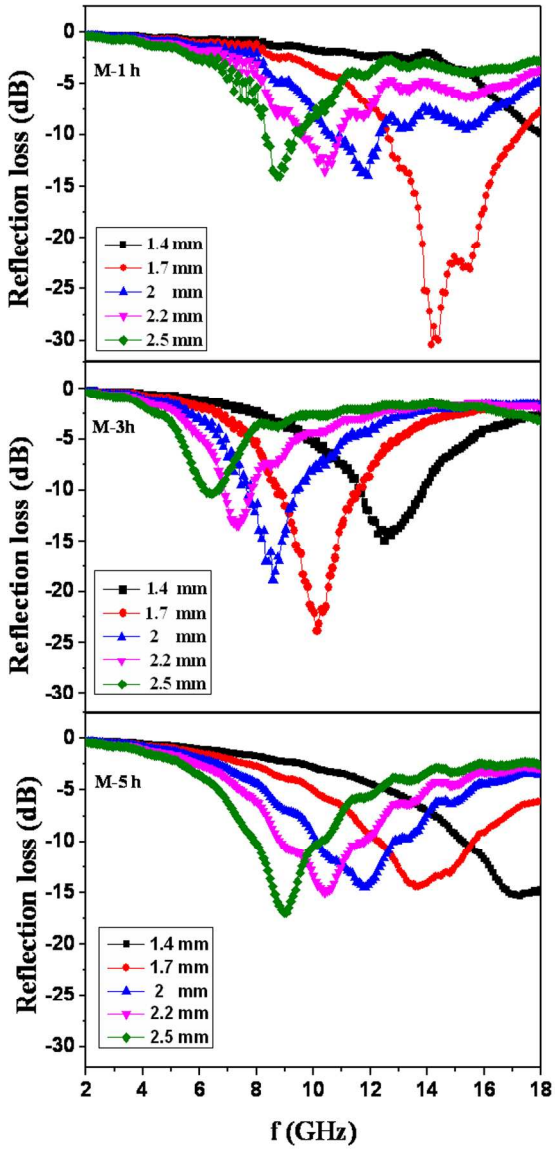

Figure 7. Microwave reflection losses of the composites coating in 2-18 GHz.
239x418mm (600 x 600 DPI)